Accepted manuscript; © IEEE Journal of Photovoltaics; final version available at DOI:10.1109/JPHOTOV.2014.2304355

Impact of Iron Precipitates on Carrier Lifetime in As-Grown and Phosphorus-Gettered Multicrystalline Silicon Wafers in Model and Experiment

Wolfram Kwapil, Jonas Schön, Florian Schindler, Wilhelm Warta, and Martin C. Schubert

***Abstract*—The impact of iron point defects on the measured injection-dependent minority carrier lifetime in silicon after different processing steps (described by the Shockley–Read–Hall equation) is well known. However, in some parts of multicrystalline silicon (mc-Si) (used for solar cells), a large share of the iron atoms is precipitated. In this study, we simulate realistic iron precipitate distributions in mc-Si after crystallization, as well as after phosphorus diffusion gettering within grains by employing the Fokker–Planck equations. Taking the Schottky contact between metallic precipitates and semiconductor into account, in a second step, we analyze the effect of recombination at iron precipitates on carrier lifetime by means of finite-element simulations. The results are compared with experimental injection-dependent lifetime measurements on a p-type mc-Si wafer before and after phosphorus diffusion. Our simulations show that in the low-lifetime edge region close to the crucible wall, a considerable share of the carrier recombination can be attributed to iron precipitates in both the as-grown and in the phosphorus-diffused state. In addition, the simulated injection dependences of iron precipitates and iron interstitials differ significantly, with the precipitates influencing the carrier lifetime especially in the mid- to high-injection range, which is supported by carrier lifetime measurements.**

***Index Terms*—Characterization of defects, charge carrier lifetime, crystalline silicon PV, finite-element methods, iron, silicon.**

I. Introduction

METALLIC precipitates in multicrystalline silicon (mc-Si) have been extensively studied in recent years. Contrary to most dissolved metal atoms, which are very effectively gettered during the phosphorus emitter diffusion, being part of the solar cell processing [1], most precipitates remain in the silicon bulk, negatively affecting the solar cell performance [2]–[4]. However, by implementing appropriate high-temperature steps, ripening of the precipitates may be effected, leading to larger but fewer metallic clusters [5]. As the recombination activity of precipitated metal atoms is in general lower than in the dissolved state [5], [6], very detailed models describing the redistribution of Fe atoms and their precipitation have been developed [7]–[11] in order to optimize processing sequences [3], [8], [11].

In this contribution, we focus on one of the most dominant impurities in mc-Si: iron [12]. During crystallization, Fe enters into the melt and the crystallized Si in high concentrations from the crucible and coating [13], [14]. In order to maintain a reasonable tradeoff between yield and cell efficiency, to a certain extent, the resulting low-lifetime edge region close to the crucible wall is accepted in industrial mc-Si wafers, having a negative impact on the mean cell efficiency of the processing lines. It can be shown that in the as-grown state, a significant fraction of the recombination activity in the low-quality edge region, as well as in the high-quality center region of mc-Si ingots, is attributed to interstitial Fe (Fe_i) [14], [15]. However, since the dissolved iron atoms are effectively removed during standard solar cell processing, one important question is to which extent precipitated Fe atoms contribute to the experimentally assessed carrier lifetime distribution before and after gettering. Knowing about the impact of Fe precipitates on lifetime would allow for further process optimization and, thus, increased cell efficiency and yield.

In several publications, the impact of the precipitate distribution on the carrier lifetime [16], [17] was calculated via the simple approach given by del Cañizo [18], which is based on the work of Hwang and Schroder [19]. However, the treatment in [18] neglects the band bending around the metallic precipitates which is a result of the internal Schottky contact between the metal cluster and the surrounding silicon [20]–[23]. According to thermionic emission theory [24], the carrier recombination at the precipitate surface depends strongly on the parameters which also affect the electric field around the precipitate, i.e., the doping concentration, the precipitate size, the Schottky barrier height, and, in particular, the injection rate [6]. A suitable approach to estimate the impact of the internal Schottky contact between precipitate and semiconductor on the carrier recombination was introduced by Plekhanov and Tan [6]. Using 1-D finite-element method (FEM) simulations, they assessed the theoretical influence of several model parameters on the recombination properties of a mean-field distribution of iron

Manuscript received September 27, 2013; revised December 2, 2013 and January 11, 2014; accepted January 20, 2014. This work was supported in part by the German Federal Ministry for the Environment, Nature Conservation, and Nuclear Safety and in part by industry partners within the research cluster "SolarWinS" under Contract 0325270G, as well as in part by the research project "THESSO" under Contract 0325491.

W. Kwapil and F. Schindler are with the Fraunhofer Institut für Solare Energiesysteme, Freiburg 79110, Germany, and also with Freiburger Materialforschungszentrum, Albert-Ludwigs-Universität Freiburg, Freiburg 79104, Germany (e-mail: wolfram.kwapil@ise.fraunhofer.de; florian.schindler@ise.fraunhofer.de).

J. Schön, W. Warta, and M. C. Schubert are with the Fraunhofer Institut für Solare Energiesysteme, Freiburg 79110, Germany (e-mail: jonas.schoen@ise.fraunhofer.de; wilhelm.warta@ise.fraunhofer.de; martin.schubert@ise.fraunhofer.de).

Color versions of one or more of the figures in this paper are available online at http://ieeexplore.ieee.org.

Digital Object Identifier 10.1109/JPHOTOV.2014.2304355

precipitates having the same radius without comparing these results to experiments. They found that "[. . .] each of [. . .] [the] conclusions holds with the other parameters [. . .] remaining constant, and should not be excessively generalized." The difficulty in finding general conclusions is a result of the interplay between the different factors mentioned previously. For example, a small precipitate that is close to a large cluster will see a different charge carrier distribution than one neighboring another small precipitate at the same distance. As a result, the space charge regions surrounding the small cluster will differ in both cases. Hence, in order to be able to compare simulated and measured recombination at precipitates, realistic distributions of iron precipitates need to be considered. As realistic Fe precipitate dimensions extend over a wide range of sizes, we use 2-D FEM simulations to accommodate both the precipitate size distribution and the wafer geometry in one model.

In the following, the carrier lifetimes due to realistic Fe precipitate distributions before and after a phosphorus emitter diffusion in two exemplary wafer regions, i.e., the wafer edge and the center part, will be analyzed. The results will be compared with carrier lifetime measurements on neighboring passivated mc-Si wafers: one in the as-grown and one in the P-diffused state. While the lifetime in the edge region can be explained by the measured interstitial iron concentration in the *low*-injection regime, we will show that it is possible to explain the relatively small slope in $\tau_{\mathrm{eff}}(\Delta n)$ at mid to high injection by the injection-dependent recombination currents toward the iron precipitates. This conclusion is valid for both the as-grown and the diffused wafer. Therefore, our model can eventually be used to evaluate the impact of Fe precipitates on solar cell parameters (e.g., via efficiency limiting bulk analysis [25]).

II. Experimental Details and Modeling

The comparison between experimental and simulated carrier lifetime values at different positions in a standard mc-Si ingot becomes possible if the iron distributions in the dissolved, as well as in the precipitated state, are known. The measurements of the total and interstitial iron distributions in the as-grown state of the exemplary wafer used for this study, as well as details concerning the crystallization process and simulations of the temperature distribution and Fe in-diffusion are presented in detail elsewhere (block named "standard" in [26] and [14]) and shall be summarized: The mc-Si crystallization of the block (format Gen1) was performed in a standard-type crucible in a laboratory crystallization furnace at Fraunhofer ISE. The p-type resistivity is around 1 Ω·cm at mid-ingot height. Total iron concentrations at the crucible wall at 50% ingot height (the position from which the wafer was taken) were determined via inductively coupled plasma mass spectrometry (ICP-MS) to be 1–3 $\times$ 10^{15} at/cm^3 after crystallization. By following a distribution resembling an error function, the values decrease to $\sim$1 $\times$ 10^{14} at/cm^3 at a distance of 2 cm to the crucible wall and to $\sim$1 $\times$ 10^{11} at/cm^3 at 4-cm distance. Interstitial iron concentrations were measured by means of Fe_i/FeB-pairing via quasi steady state photoluminescence (QSSPL)–calibrated photoluminescence (PL) imaging [26], [27] on as-cut wafers to be around 1 $\times$ 10^{12} at/cm^3 in the edge region and around 1 $\times$ 10^{11} at/cm^3 in the center region.

Prior to the QSSPL measurements, the wafers were surface-passivated by $\mathrm{Al_2O_3}$ atomic layer deposition, allowing for very low-surface recombination velocities. On FZ reference wafers, lifetimes above 1 ms in the entire injection range of interest were achieved. While we expect no influence on carrier lifetime because of passivation of defects by hydrogen atoms diffusing from the passivation layer, a slight growth of the precipitates because of the low-temperature anneal needed for surface passivation activation may have occurred, slightly increasing the carrier lifetime. However, we estimate this uncertainty to be negligible in comparison with other sources of error discussed next because of the short times needed for this process step. Care was taken to separate the Fe_i/FeB-metastability from other metastable defects like the formation of the B–O complex or the Cr_i/CrB defects by following the procedure described in [27].

A phosphorus emitter diffusion at 825 °C was applied to a neighboring wafer. After emitter etch-back and $\mathrm{Al_2O_3}$ surface passivation, the interstitial iron concentration was measured to be approximately 3 $\times$ 10^{11} at/cm^3 in the edge region and $\sim$1 $\times$ 10^{10} at/cm^3 in the wafer center [15]. As the total iron concentration after diffusion could not be determined via ICP-MS, we rely on the simulations of the Fe redistribution during the high-temperature step, which will be explained in detail next.

The electron-hole recombination at the precipitate surface depends on the electric field strength and, hence—beside other factors—on the precipitate size. For our study, we thus need detailed information about the precipitate size distribution as a function of the distance to the crucible wall. Unfortunately, these data are not accessible on a statistical scale via experiments (particularly along dislocation lines crossing the wafer bulk), e.g., by means of micro-X-ray fluorescence [28]. Therefore, we use 2-D simulations (Sentaurus Process [29]), which yield—besides the Fe_i concentration—the distribution of the Fe cluster sizes (for details, see [3], [9], and [11]). As shown in [14], our simulations could reproduce the measured total and interstitial iron distributions as a function of the distance to the crucible wall in the as-grown wafer taken for this study with high accuracy.

The 2-D Fe distribution simulation is based on the diffusion equations and the Fokker–Planck equations. As input, a 2-D symmetry element containing the interface between the crucible wall and the mc-Si crystal is given together with a typical dislocation distribution [14]. The dislocations are assumed to be perpendicular to the 2-D plane. In the model, the dislocations serve as nucleation sites for Fe precipitation. In addition, the entire temperature ramp during crystallization is considered and used for the calculation of impurity in-diffusion into the melt, as well as into the solidified crystal and the nucleation and precipitation process, yielding the precipitate distribution in the as-grown state. In the calculation of the distribution after the phosphorus diffusion, in addition the gettering effect is taken into account [11]. In [3], simulation results of mc-Si in the as-grown, as well as in the phosphorus-gettered state, were compared with X-ray fluorescence microscopy (μ-XRF) measurements of Fe clusters along grain boundaries,

and a reasonable agreement was found. In addition, measured changes in Fe_i concentration because of dissolution and precipitation, as well as the gettering effects, were reproduced with simulations providing evidence for the soundness of this approach [11], [15].

Since the heterogeneous precipitation of iron depends very sensitively on the temperature history of the silicon samples, the largest contribution to the uncertainty in the predicted precipitate size density comes from the temperature ramp during crystallization. Unfortunately, direct *in-situ* temperature measurements in the bulk silicon are impossible. Hence, complex simulations of the temperature fields in the crystallization furnace and the silicon block, incorporating diffusive and convective mass transport in the melt and the atmosphere, were used for the precipitation simulations [14]. A second source of uncertainty comes from the measurement of the distance between the crucible wall and the edge of the wafer taken from approximately 50% ingot height that was used for carrier lifetime measurements, the precipitate size distribution in the wafer edge being strongly dependent on the distance to the crucible wall.

In this study, we are interested in the reasons for limitations of the carrier lifetime in the low-lifetime edge region as compared with the wafer center region. Understanding the limitations may help to optimize process sequences in order to increase the carrier lifetime in the edge region, which has severely affected the material performance up to now. The greatest lifetime enhancement is likely within the grains with low dislocation densities [1]. Therefore, in the following, we disregard grain boundaries and regions of high dislocation density $\rho_{\mathrm{DL}} \geq 10^5$ cm^{-2} and focus on the carrier lifetime inside grains (background dislocation density $\rho_{\mathrm{DL}} \sim 10^4$ cm^{-2}). Fe nucleation in grains far away from a grain boundary occurring most likely at the remaining dislocations [30], [31], we assume that the precipitates are aligned along a dislocation line traversing the entire wafer thickness. Taking a relatively low ρ_{DL} of 1×10^4 cm^{-2}, we can calculate the number of precipitates of a certain size expected to be found at the dislocation, which we use for the following calculation.

The simulations of the injection-dependent precipitate-related carrier lifetime are based on 2-D axisymmetric finite-element simulations using Comsol Multiphysics. A sketch of the model geometry and some of the basic features is presented in Fig. 1 (on the left). The simulation domain is bounded by the wafer surfaces (top and bottom), the wafer thickness being 200 μm, and the domain radius equals 56.42 μm (which corresponds to a ρ_{DL} of 10^4 cm^{-2}). The spherical precipitates of different size and number are aligned along the axis of symmetry representing the dislocation line. The precipitates are randomly distributed in size along the dislocation. Between neighboring precipitates, an equal distance is maintained. An electron-hole generation profile G correlating with AMG1.5 g spectrum illumination is used. Besides recombination at the wafer surfaces and at the precipitates, band-to-band recombination R_{BB} (parameterization from [32]), Auger recombination R_{Auger} [33], and Shockley–Read–Hall recombination at iron interstitials R_{Fei} [34] are taken into account.

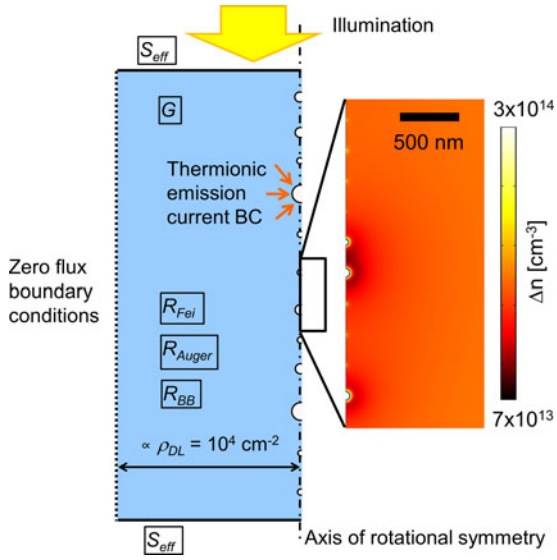

Fig. 1. Left: Sketch of the model structure (not to scale) used in the FEM simulations of recombination currents at internal Schottky contacts (thermionic emission current BCs between Fe precipitates and silicon and (right) exemplary zoom into the simulated steady-state minority carrier distribution (generation rate 1 sun), shown for the precipitate size density labeled "egde–distr. 1" (see Fig. 3). Moving from the precipitate–semiconductor interface toward the Si bulk, a minority carrier accumulation is followed by a depleted region before the bulk average minority carrier concentration is attained. Interplay between neighboring precipitates can be exemplarily seen in the overlapping minority carrier reduction in the vicinity of the two large precipitates close to the middle of the image.

The simulation is based on the approach that is presented in previous publications by Plekhanov and Tan [6] and by Negoita and Tan [35], and the details of the derivation of the boundary condition (BC) equations and the implementation can also be found in [6] and [35]. In the following, the implementation used in this study is summarized.

In the silicon bulk, the simulation solves the continuity equations for electrons and holes and the Poisson equation (assuming Maxwell–Boltzmann statistics) with the three unknown variables Φ_e, Φ_h, and Ψ, i.e., the quasi-Fermi potentials for electrons and holes and the electrostatic potential, respectively. At the wafer surfaces, recombination fluxes corresponding to a surface recombination velocity $S_{\mathrm{eff}} = 200$ cm/s are chosen as Neumann BC, while the boundaries perpendicular to the wafer surface are described by zero flux BCs, assuming lateral periodicity.

As described in [6] and [35], the interface between silicon and the metallic precipitates is assumed to represent an internal Schottky contact that is described by the Schottky barrier Φ_B. We suppose the precipitates to consist of iron silicide (FeSi) with the Schottky barrier $\Phi_B = 0.68$ eV (p-type Si) [6]. As will be shown next, realistic precipitate distributions extend over a wide range of sizes from several atoms per cluster (radius < 1 nm) to precipitate radii of several tens of nanometers. It is likely that the electronic properties and, therefore, the Schottky barrier height depend on the precipitate size for example due to quantum mechanical effects [20] or due to lattice misfit effects that induce stress for larger clusters [36]. However, for precipitates above a

certain size, we expect the change in Schottky barrier height to be relatively small, which, according to Plekhanov and Tan [6], should have a negligible impact on the recombination activity. For small precipitates with radii in the order of 0.1 to 1 nm, the change in Schottky barrier height may be significant, or the Schottky contact model may even not be valid at all. In the next section, we will show that the contribution of these precipitates to the total recombination is negligible. Hence, we expect the error that is introduced by approximating the Schottky barrier height by a single value to be small.

The Schottky contact results in thermionic emission current densities of electrons j_e and holes j_h:

$$j_e = A_e^* T^2 \exp\left(-\frac{q\Phi_B}{k_B T}\right)\left\{\exp\left(\frac{-q\Phi_e - E_{F,m}}{k_B T}\right) - 1\right\} \quad (1)$$

$$j_h = A_h^* T^2 \exp\left(-\frac{E_G - q\Phi_B}{k_B T}\right)\left\{\exp\left(\frac{q\Phi_h + E_{F,m}}{k_B T}\right) - 1\right\}. \quad (2)$$

Here, $A_{e,h}^*$ signifies the effective Richardson constants for electrons and holes, respectively, T the temperature, q the elementary charge, k_B the Boltzmann constant, E_G the band gap of silicon, and $E_{F,m}$ the Fermi level in the iron precipitates. The precipitates charge with the majority carrier species and a depletion region surrounding the metal cluster evolves, attracting minority carriers and repelling majority carriers [35]. In thermodynamic equilibrium (in the dark), the net fluxes of electrons and holes toward the precipitates are zero [35]. Under injection conditions, e.g., illumination, the strong electric fields in the depletion regions around the precipitates decrease [35]. As a consequence, both electrons and holes travel toward the precipitates where they recombine [35]. In the steady state, electron and hole current densities at the precipitate–Si interface must be in equilibrium:

$$j_e|_{\text{interface}} = j_h|_{\text{interface}}\,. \quad (3)$$

Here, it is assumed that the recombination velocity is not the limiting factor once the carriers reach the Fe precipitate surface [6].

The condition (3), together with (1) and (2), is used to derive a consistent set of BCs describing the recombination at metallic precipitates [35].

Because of the charging of the precipitates, large electric fields evolve which can reach up to several 10^6 V/cm. In particular, this is the case for small precipitates and very low injection. In this high-field regime, the carrier mobility, for which we use Klaassen's model [37], [38], has to be corrected for field effects [39].

From the primary result of these simulations—the spatial distribution of the potentials Φ_e, Φ_h, and Ψ—all necessary values can be derived. In particular, the excess minority carrier density Δn is obtained by averaging the electron concentration over the whole simulation domain. The recombination due to the precipitates is calculated by integrating the recombination currents over the interfaces of all precipitates, yielding the total recombination rate R_{prec}, which is then averaged over the whole simulation domain.

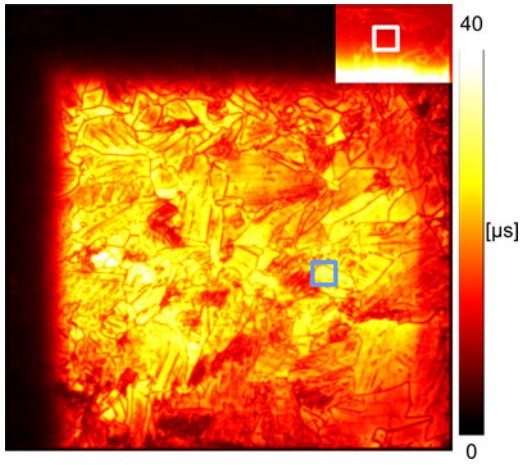

Fig. 2. Carrier lifetime at a generation rate of 0.1 sun on the passivated as-grown wafer taken from approximately 50% ingot height showing low-lifetime edge regions at the upper and left sides. Scaling is linear, 0 to 40 μs, for the image of the entire wafer. The white rectangle marks the ROI from which the measured injection-dependent carrier lifetime was extracted (see Fig. 4). In the blue rectangle, the carrier lifetime in the "center" was evaluated. The inset in the edge to the upper right is scaled to 0–5 μs in order to highlight the ROI in the edge region.

As usual, the quasi-steady state carrier lifetime $\tau_i(\Delta n)$ that is related to the recombination rate channels R_i is calculated as

$$\tau_i\left(\Delta n\right) = \frac{\Delta n}{R_i} \quad (4)$$

with i symbolizing the recombination channel.

III. Results

In Fig. 2, the QSSPL-calibrated PL image of the as-grown wafer taken for this study is shown. In both the as-grown and the phosphorus-diffused sister wafer, two exemplary regions of interest (ROI) were chosen, which are marked by the rectangles: The first one represents a grain with low dislocation density in the low-lifetime edge region that is approximately 15–20 mm away from the crucible wall. For the second ROI, a grain of relatively good crystal quality possessing a low dislocation density in the center region of the ingot was chosen. Care was taken to average only over pixels with a significant distance to the surrounding grain boundaries. In order to avoid possible influences of light-spreading effects on the carrier lifetime measurements [40] in P-diffused wafers because of the large intensity difference between center and edge, here, the high-lifetime center region was masked out, and the QSSPL measurement approach in [41] was used. In general, we estimate the carrier lifetime measurement error to be $\sim$20%.

In Fig. 3, the simulated Fe cluster size densities inside the grains in the edge ROI and in the good wafer area ROI which were taken as input for the calculation of the carrier lifetime are shown. For the evaluation, cluster sizes (number of atoms per

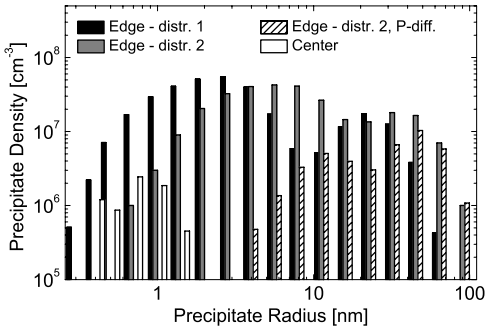

Fig. 3. Distribution of the precipitate size density within the grains in the edge before (black and gray) and after phosphorus diffusion (shaded white) as well as in the center (white) regions at 50% ingot height taken from simulations of mc-Si crystallization [10], [14]. The distribution in the edge region labeled with "distr. 1" corresponds to a grain 15–20 mm away from the crucible wall that was cooled down with the simulated temperature profile (see the marked edge region in Fig. 2). The distribution 2 represents a ROI closer to the crucible wall and was used for uncertainty estimations (see the text).

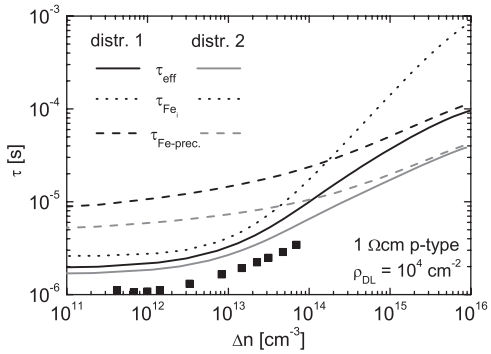

Fig. 4. Calculation of the carrier lifetime (in the dissociated state) in the edge region before phosphorus diffusion where the Fei concentration was measured to be 1×10^{12} at/cm^3. The measured increase of the carrier lifetime with the increasing injection level (black symbols) is smaller than expected if only the SRH recombination at dissolved iron atoms (dotted line) is accounted for. However, taking recombination at Fe precipitates (dashed lines) into account, the calculated effective lifetime (continuous lines) agrees well with measurements. For the explanation of the difference in gray and black lines, please refer to the text.

cluster) were binned exponentially. The four different precipitate size densities investigated in this study are detailed as follows:

1) "Edge–distr. 1" (black columns) represents the precipitate distribution inside the grains in the edge ROI in the as-grown state, 15–20 mm away from the crucible wall.
2) "Edge–distr. 2" (gray columns) features a higher density of larger Fe clusters compared with the previous distribution, which is found closer to the crucible wall because of the higher total Fe concentration. Larger precipitates may also result from a smaller cooling rate after crystallization. Hence, by this distribution variation in the as-grown state, we estimate the impact of the uncertainties in Fe precipitate distribution mentioned in the previous section.
3) "Edge–distr. 2, P-diff." (white-shaded columns) represents the simulated Fe precipitate distribution inside grains in the edge after a phosphorus emitter diffusion (gettering) step.
4) "Center" (white columns) stands for a typical simulated Fe cluster distribution inside grains in the good wafer area far away from the crucible wall.

While the Fe in-diffusion from crucible and coating during the cool down leads to a high precipitate density and to a significant fraction of large precipitates in the edge region, in the ingot center, only few and relatively small precipitates are to be expected. During the phosphorus diffusion, the change in the Fe cluster distribution depends strongly on the precipitate size: While small precipitates are effectively dissolved because of the high temperature, large precipitates are hardly affected. After P-diffusion, most of the dissolved iron atoms are gettered or reprecipitated at the remaining clusters.

An example for the simulated steady-state minority carrier distribution taking the thermionic emission currents into account is presented in Fig. 1 (on the right). Depending on the precipitate size density and the properties which have an influence on the electric field, precipitates can interact via overlapping space charge regions.

The measurements of the injection-dependent carrier lifetime that is averaged according to a square-root harmonic mean within the edge ROI before P-diffusion are presented in Fig. 4. The lifetime in the edge region increases from 1 μs in low injection to 3 μs in the mid-injection range. These experimental values can only partly be explained by SRH recombination at iron interstitials of the measured (and simulated [14]) concentrations of 1×10^{12} at/cm^3 in this region. In particular, in the mid- to high-injection regime, significant deviations occur.

As shown in Fig. 4, the calculated recombination at Fe precipitates (dashed lines) shows a notable injection dependence, which has a slighter slope than the SRH recombination channel for Fe$_i$. With the Fe-precipitate size distribution expected for the edge part of the ingot, our calculations show that recombination at precipitates dominates the carrier lifetime starting at an injection level of around 5×10^{13} to 1×10^{14} cm^{-3}. Hence, one possible explanation for the relatively slow increase in measured effective carrier lifetime in mid- to high-injection is the presence of Fe clusters.

The difference between measurement and simulation with the second set (grey continuous line) amounts to 0.5–1.5 μs (for 1×10^{11} cm$^{-3} < \Delta n < 1 \times 10^{14}$ cm^{-3}) and remains small. In this example, only a small fraction of the measured total recombination at additional centers, apart from iron-related ones, has to be assumed in order to reach perfect agreement. The good agreement, supposing a higher concentration of large precipitates, gives support to the hypothesis that the injection-dependent lifetime in the edge region can be attributed in a large part to recombination at iron interstitials (being prominent in the low-injection range) and recombination at Fe precipitates (important in the mid- to high-injection range).

Of course, also other impurities like Cu, Ni, O, etc., are present in the wafer. However, the carrier lifetime distribution as a function of the distance to the crucible wall follows a profile that provides a fingerprint of the diffusion length (dependent on crystallization conditions) of the limiting defect. The distribution of most other impurities is different because of their different diffusivity; for example, the concentration of Cu and Ni is

laterally almost homogeneous [13] because of their large diffusion length [42], which levels out any gradients during cooldown. Therefore, the impact of these elements on carrier lifetime can theoretically be observed in the wafer center region as well. Since the carrier lifetimes in the wafer center and the edge differ strongly, it is unlikely that these impurities contribute significantly to the lifetime limitation in the wafer edge region. This line of reasoning applies to most of other impurity elements [42]. Of course, our measurements in the wafer edge ROI still contain the influence of impurities with diffusivity similar to Fe, like, e.g., Cr, which are not regarded in the simulations.

During measurements of the dissolved Fe concentration via the Fe_i/FeB metastability [43], the injection dependence of precipitate-related lifetime needs to be considered if the Fe concentration is high and the precipitate density is significant (in particular in the wafer edge regions). Since the [Fe_i] evaluation assumes that the measured effective lifetime has no other injection dependence than one introduced by the Fe_i/FeB defect, it is advisable to choose an injection level in which the precipitate-related carrier lifetime is almost constant. Our simulations suggest this to be the case at low-minority carrier densities roughly below 5×10^{12} cm^{-3}.

Comparing our results to previous approximations of the precipitate-related carrier lifetime, the estimation that is based on the equations in [18] and [19] for the precipitate size distributions yields 44.4 μs and 14.9 μs for distributions 1 and 2, respectively. In our calculations, these values are expected to be found only at an injection level around 5×10^{14} cm^{-3} (corresponding to $\sim$1.7 and $\sim$3 suns, respectively), with significantly lower lifetime values at lower injection. Depending on the injection conditions, the values that were estimated by the approach in [18] may differ from the real values by an order of magnitude. The reason is that the simple approach neglects the space charge region around the precipitates, which also depends on the injection conditions.

During phosphorus diffusion, in the edge region, small precipitates are effectively dissolved, and a large part of the interstitial iron atoms are gettered (the remaining Fe_i concentration being approx. 3×10^{11} at/cm^3). However, with increasing precipitate size, the effect of the P-diffusion decreases. The resulting simulations of the carrier lifetime after P-diffusion, as well as the measured lifetime on the P-diffused sister wafer, are shown in Fig. 5. The simulation is in reasonable agreement with the measured lifetime, which increases during P-diffusion by a factor of $\sim$2–3, depending on injection density. Again, we attribute the deviation between simulation and measurement mainly to the uncertainty in the precipitate size distribution. While Fe interstitials still play a significant role in the low-injection regime, the precipitates mainly limit the carrier lifetime above an injection level $>1 \times 10^{13}$ cm^{-3}. After P-diffusion, the relative impact of Fe precipitates on lifetime increases strongly compared with the as-grown state, because of the lower Fe_i concentration. For example, at an injection level of 1×10^{14} cm^{-3}, from our calculations, we estimate the share of recombination at precipitates to be roughly 40% of the total recombination before P-diffusion. After emitter diffusion, we attribute about 70% of the total recombination to the influence of Fe precipitates. This example shows how important it is to consider the effect of Fe precipitates in the edge region during solar cell processing.

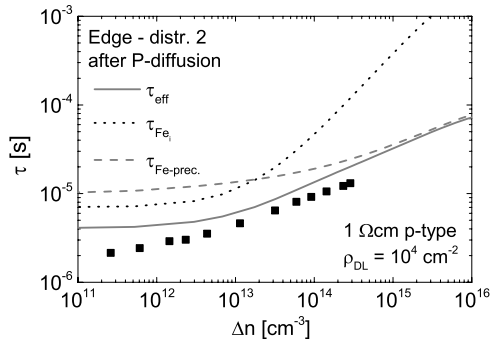

Fig. 5. Calculation of the carrier lifetime after phosphorus diffusion in the edge region ($Fe_i \sim 3 \times 10^{11}$ at/cm^3) assuming the precipitate distribution 2. The simulation shows the same trend as the lifetime measurement (black symbols), indicating that in the wafer edge, the remaining precipitates may play a significant role.

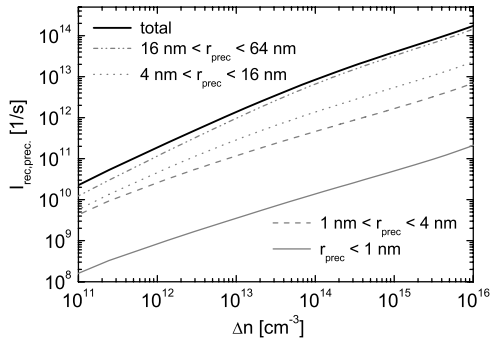

Fig. 6. Injection-dependent recombination current for precipitates with different sizes, exemplarily shown for the precipitate distribution 1. The gray lines represent the recombination currents integrated over all precipitates with sizes mentioned in the legend. Recombination at the large precipitates is predominant; hence, in principle, precipitates with radii $<$4 nm can be neglected. The black continuous line represents the total precipitate-related recombination current.

In the good wafer region inside the grains, we calculate a Fe precipitate-related lifetime above 1 ms (not shown), which means that Fe precipitates of the simulated size distribution labeled "center" in Fig. 3 do not affect the carrier lifetime independent of the injection density. The measured lifetimes in the as-grown state can be well explained by recombination at iron interstitials at least in the low- to mid-injection regime. A difference between measured effective carrier lifetime and Fe_i recombination in the mid- to high-injection range is observed, which we attribute to other background defects.

A deeper analysis of the four exemplary simulations presented previously reveals that at least for the precipitate distributions assumed herein, recombination at large precipitates is predominant, where the influence of small precipitates with radii roughly below 4 nm is negligible (see Fig. 6). This explains the noticeable difference between precipitate distributions of significantly different sizes (edge–distr. 1 and 2; see Fig. 4). Obtaining a large lifetime increase in the wafer edge region by a simple phosphorus emitter diffusion/gettering is challenging because large precipitates are the most difficult to getter and, at the same time, have the largest impact on lifetime.

IV. Conclusion

Metal precipitates in mc-Si, with iron clusters being the most prominent of all because of the high Fe concentration in the crucible and coating, significantly reduce the carrier lifetime, the metallic silicides likely forming an internal Schottky contact with the surrounding silicon. The resulting thermionic emission currents (recombination currents) depend on all parameters which have an impact on the electric field around the precipitates, in particular the injection level.

Our simulations of realistic precipitate size densities and recombination of charge carriers at precipitates at a low dislocation density show that a possible explanation for the measured injection-dependent carrier lifetime is that in the mid- to high-injection range in the grains of the edge region close to the crucible wall is limited by recombination at iron precipitates, while SRH recombination at iron interstitials plays a crucial role only at low injection. Our results therefore indicate that the internal Schottky contact at the iron precipitate interfaces has to be taken into account in order to understand and predict the injection-dependent carrier lifetime at least in the wafer edge correctly. Calculations of precipitate-related recombination inside the grains in the wafer edge after a phosphorus diffusion step, which leads to the dissolution of the small precipitates and gettering of most of the interstitial iron and, thus, to a slight lifetime increase, are also in good accordance with measurements.

In our simulations, the precipitate-related recombination is dominated by the large precipitates with radii >4 nm. Since large iron clusters are hardly dissolved during standard gettering steps, their relative impact on the lifetime increases considerably during processing.

Within grains in the wafer center, no impact of Fe clusters on carrier lifetime is expected.

By combining realistic simulations of the precipitate size density evolution during crystallization and processing with calculations of the recombination at the precipitate surfaces, we are now able to estimate the impact of various process sequences on one of the most important material parameters in solar cell processing: the carrier lifetime (diffusion length).

Acknowledgment

The authors would like to thank A. Abdollahinia for assistance with the precipitate distribution simulations, as well as L. Mundt and J. Giesecke for the carrier lifetime measurements.

References

[1] A. Bentzen, A. Holt, R. Kopecek, G. Stokkan, J. S. Christensen, and B. G. Svensson, "Gettering of transition metal impurities during phosphorus emitter diffusion in multicrystalline silicon solar cell processing," *J. Appl. Phys.*, vol. 99, pp. 093509-1–093509-6, 2006.

[2] D. P. Fenning, J. Hofstetter, M. I. Bertoni, S. Hudelson, M. Rinio, J. F. Lelièvre, B. Lai, C. Del Cañizo, and T. Buonassisi, "Iron distribution in silicon after solar cell processing: Synchrotron analysis and predictive modeling," *Appl. Phys. Lett.*, vol. 98, pp. 162103-1–162103-3, 2011.

[3] J. Schön, A. Haarahiltunen, H. Savin, D. P. Fenning, T. Buonassisi, W. Warta, and M. C. Schubert, "Analyses of the evolution of iron-silicide precipitates in multicrystalline silicon during solar cell processing," *IEEE J. Photovoltaics*, vol. 3, no. 1, pp. 131–137, Jan. 2013.

[4] D. P. Fenning, J. Hofstetter, M. I. Bertoni, G. Coletti, B. Lai, C. Del Cañizo, and T. Buonassisi, "Precipitated iron: A limit on gettering efficacy in multicrystalline silicon," *J. Appl. Phys.*, vol. 113, pp. 044521-1–044521-12, 2013.

[5] T. Buonassisi, A. A. Istratov, M. A. Marcus, B. Lai, Z. Cai, S. M. Heald, and E. R. Weber, "Engineering metal-impurity nanodefects for low-cost solar cells," *Nat. Mater. Lett.*, vol. 4, pp. 676–679, 2005.

[6] P. S. Plekhanov and T. Y. Tan, "Schottky effect model of electrical activity of metallic precipitates in silicon," *Appl. Phys. Lett.*, vol. 76, no. 25, pp. 3777–3779, 2000.

[7] A. Haarahiltunen, H. Väinölä, O. Anttila, E. Saarnilehto, M. Yli-Koski, J. Storgårds, and J. Sinkkonen, "Modeling of heterogeneous precipitation of iron in silicon," *Appl. Phys. Lett.*, vol. 87, pp. 151908-1–151908-4, 2005.

[8] A. Haarahiltunen, H. Väinölä, and M. Yli-Koski, "Modeling and optimization of internal gettering of iron in silicon," *ECS Trans.*, vol. 3, no. 4, pp. 273–284, 2006.

[9] A. Haarahiltunen, H. Väinölä, O. Anttila, M. Yli-Koski, and J. Sinkkonen, "Experimental and theoretical study of heterogeneous iron precipitation in silicon," *J. Appl. Phys.*, vol. 101, pp. 043507-1–043507-6, 2007.

[10] J. Schön, H. Habenicht, M. C. Schubert, and W. Warta, "Simulation of iron distribution after crystallization of mc silicon," *Solid State Phenomena*, vol. 156–158, pp. 223–228, 2010.

[11] J. Schön, H. Habenicht, M. C. Schubert, and W. Warta, "Understanding the distribution of iron in multicrystalline silicon after emitter formation: theoretical model and experiments," *J. Appl. Phys.*, vol. 109, pp. 063717-1–063717-8, 2011.

[12] D. Macdonald, A. Cuevas, A. Kinomura, Y. Nakano, and L. J. Geerligs, "Transition-metal profiles in a multicrystalline silicon ingot," *J. Appl. Phys.*, vol. 97, pp. 033523-1–033523-7, 2005.

[13] W. Kwapil, A. Zuschlag, I. Reis, I. Schwirtlich, S. Meyer, R. Zierer, R. Krain, F. K. Kießling, M. Schumann, C. Schmid, and S. Riepe, "Influence of crucible and coating on the contamination of directionally solidified silicon: First results of the German research network SolarWinS," in *Proc. 27th Eur. Photovoltaics Sol. Energy Conf. Exhib.*, Frankfurt, Germany, 2012, pp. 627–635.

[14] M. C. Schubert, J. Schön, F. Schindler, W. Kwapil, A. Abdollahinia, B. Michl, S. Riepe, C. Schmid, M. Schumann, S. Meyer, and W. Warta, "Impact of impurities from crucible and coating on mc-silicon quality—The example of iron and cobalt," *IEEE J. Photovoltaics*, vol. 3, no. 4, pp. 1250–1258, Oct. 2013.

[15] F. Schindler, B. Michl, J. Schön, W. Kwapil, W. Warta, and M. C. Schubert, "Solar cell efficiency losses due to impurities from the crucible in multicrystalline silicon," *IEEE J. Photovoltaics*, vol. 4, no. 1, pp. 122–129, Jan. 2014.

[16] M. C. Schubert, J. Schön, B. Michl, A. Abdollahinia, and W. Warta, "Modeling distribution and impact of efficiency limiting metallic impurities in silicon solar cells," in *Proc. IEEE 38th Photovoltaic Spec. Conf.*, Austin, TX, USA, 2012, pp. 286–291.

[17] M. C. Schubert, J. Schön, B. Michl, A. Abdollahinia, and W. Warta, "Advances in characterization and modeling of efficiency limiting impurities in silicon solar cells," presented at the 6th Int. Symp. Adv. Sci. Technol Silicon Mater., Kona, HI, USA, Nov. 19–23, 2012.

[18] C. Del Cañizo and A. Luque, "A comprehensive model for the gettering of lifetime-killing impurities in silicon," *J. Electrochem. Soc.*, vol. 147, no. 7, pp. 2685–2692, 2000.

[19] J. M. Hwang and D. K. Schroder, "Recombination properties of oxygen-precipitated silicon," *J. Appl. Phys.*, vol. 59, pp. 2476–2487, 1986.

[20] A. Broniatowski, "Multicarrier trapping by copper microprecipitates in silicon," *Phys. Rev. Lett.*, vol. 62, pp. 3074–3077, 1989.

[21] C. Donolato, "The space-charge region around a metallic platelet in a semiconductor," *Semicond. Sci. Technol.*, vol. 8, pp. 45–49, 1993.

[22] P. Formanek and M. Kittler, "Direct evidence of internal Schottky barriers at NiSi2 precipitates in silicon by electron holography," *J. Appl. Phys.*, vol. 97, pp. 063707-1–063707-5, 2005.

[23] M. Kittler, J. Lärz, W. Seifert, M. Seibt, and W. Schröter, "Recombination properties of structurally well defined $NiSi_2$ precipitates in silicon," *Appl. Phys. Lett.*, vol. 58, pp. 911–913, 1991.

[24] C. Herring and M. H. Nichols, "Thermionic emission," *Rev. Mod. Phys.*, vol. 21, no. 2, pp. 185–270, 1949.

[25] B. Michl, M. Rüdiger, J. Giesecke, M. Hermle, W. Warta, and M. C. Schubert, "Efficiency limiting bulk recombination in multicrystalline silicon solar cells," *Sol. Energy Mater. Sol. Cells*, vol. 98, pp. 441–447, 2012.

[26] D. Macdonald, J. Tan, and T. Trupke, "Imaging interstitial iron concentrations in boron-doped crystalline silicon unsing photoluminescence," *J. Appl. Phys.*, vol. 103, pp. 073710-1–073710-7, 2008.
[27] M. C. Schubert, H. Habenicht, and W. Warta, "Imaging of metastable defects in silicon," *IEEE J. Photovoltaics*, vol. 1, no. 2, pp. 168–173, Oct. 2011.
[28] M. I. Bertoni, D. P. Fenning, M. Rinio, V. Rose, M. Holt, J. Maser, and T. Buonassisi, "Nanoprobe X-ray fluorescence characterization of defects in large-area solar cells," *Energy Environ. Sci.*, vol. 4, pp. 4252–4257, 2011.
[29] *Sentaurus TCAD*, Synopsys, Zürich, Switzerland, 2010.
[30] J. Bailey, S. A. McHugo, H. Hieslmair, and E. R. Weber, "Efficiency-limiting defects in silicon solar cell material," *J. Electron. Mater.*, vol. 25, pp. 1417–1421, 1996.
[31] S. A. McHugo, A. C. Thompson, G. Lamble, C. Flink, and E. R. Weber, "Metal impurity precipitates in silicon: chemical state and stability," *Physica B*, vol. 273–274, pp. 371–374, 1999.
[32] M. A. Green, *Solar Cells: Operating Principles, Technology And System Applications*. Kensington, Australia: Univ. New South Wales, 1986, ch. 3, p. 52.
[33] J. Dziewior and W. Schmid, "Auger coefficients for highly doped and highly excited silicon," *Appl. Phys. Lett.*, vol. 31, pp. 346–348, 1977.
[34] A. A. Istratov, H. Hieslmair, and E. R. Weber, "Iron and its complexes in silicon," *Appl. Phys. A, Mater. Sci. Process.*, vol. 69, pp. 13–44, 1999.
[35] M. D. Negoita and T. Y. Tan, "Metallic precipitate contribution to generation and recombination currents in p-n junction devices due to the Schottky effect," *J. Appl. Phys.*, vol. 94, pp. 5064–70, 2003.
[36] J. D. Murphy, K. Bothe, M. Olmo, V. V. Voronkov, and R. J. Falster, "The effect of oxide precipitates on minority carrier lifetime in p-type silicon," *J. Appl. Phys.*, vol. 110, pp. 053713-1–053713-9, 2011.
[37] D. B. M. Klaassen, "A unified mobility model for device simulation—I. Model equations and concentration dependence," *Solid State Electron.*, vol. 35, pp. 953–959, 1992.
[38] D. B. M. Klaassen, "A unified mobility model for device simulation—II. Temperature dependence of carrier mobility and lifetime," *Solid State Electron.*, vol. 35, pp. 961–967, 1992.
[39] C. Canali, G. Majni, R. Minder, and G. Ottaviani, "Electron and hole drift velocity measurements in silicon and their empirical relation to electric field and temperature," *IEEE Trans. Electron Devices*, vol. ED-22, no. 11, pp. 1045–1047, Nov. 1975.
[40] D. Walter, A. Fell, E. Franklin, D. Macdonald, B. Mitchell, and T. Trupke, "The impact of Silicon CCD photon spread on quantitative analyses of luminescence images," *IEEE J. Photovoltaics*, vol. 4, no. 1, pp. 368–373, Jan. 2014.
[41] J. A. Giesecke, T. Niewelt, M. Rüdiger, M. Rauer, M. C. Schubert, and W. Warta, "Broad range injection-dependent minority carrier lifetime from photoluminescence," *Sol. Energy Mater. Sol. Cells*, vol. 102, pp. 220–224, 2012.
[42] K. Graff, *Metal Impurities in Silicon-Device Fabrication*, 2nd ed. Berlin, Germany: Springer, 2000.
[43] G. Zoth and W. Bergholz, "A fast, preparation-free method to detect iron in silicon," *J. Appl. Phys.*, vol. 67, pp. 6764–6771, 1990.

Authors' photographs and biographies not available at the time of publication.

Impact of Iron Precipitates on Carrier Lifetime in As-Grown and Phosphorus-Gettered Multicrystalline Silicon Wafers in Model and Experiment

Wolfram Kwapil, Jonas Schön, Florian Schindler, Wilhelm Warta, and Martin C. Schubert

***Abstract*—The impact of iron point defects on the measured injection-dependent minority carrier lifetime in silicon after different processing steps (described by the Shockley–Read–Hall equation) is well known. However, in some parts of multicrystalline silicon (mc-Si) (used for solar cells), a large share of the iron atoms is precipitated. In this study, we simulate realistic iron precipitate distributions in mc-Si after crystallization, as well as after phosphorus diffusion gettering within grains by employing the Fokker–Planck equations. Taking the Schottky contact between metallic precipitates and semiconductor into account, in a second step, we analyze the effect of recombination at iron precipitates on carrier lifetime by means of finite-element simulations. The results are compared with experimental injection-dependent lifetime measurements on a p-type mc-Si wafer before and after phosphorus diffusion. Our simulations show that in the low-lifetime edge region close to the crucible wall, a considerable share of the carrier recombination can be attributed to iron precipitates in both the as-grown and in the phosphorus-diffused state. In addition, the simulated injection dependences of iron precipitates and iron interstitials differ significantly, with the precipitates influencing the carrier lifetime especially in the mid- to high-injection range, which is supported by carrier lifetime measurements.**

***Index Terms*—Characterization of defects, charge carrier lifetime, crystalline silicon PV, finite-element methods, iron, silicon.**

I. Introduction

METALLIC precipitates in multicrystalline silicon (mc-Si) have been extensively studied in recent years. Contrary to most dissolved metal atoms, which are very effectively gettered during the phosphorus emitter diffusion, being part of the solar cell processing [1], most precipitates remain in the silicon bulk, negatively affecting the solar cell performance [2]–[4]. However, by implementing appropriate high-temperature steps, ripening of the precipitates may be effected, leading to larger but fewer metallic clusters [5]. As the recombination activity of precipitated metal atoms is in general lower than in the dissolved state [5], [6], very detailed models describing the redistribution of Fe atoms and their precipitation have been developed [7]–[11] in order to optimize processing sequences [3], [8], [11].

In this contribution, we focus on one of the most dominant impurities in mc-Si: iron [12]. During crystallization, Fe enters into the melt and the crystallized Si in high concentrations from the crucible and coating [13], [14]. In order to maintain a reasonable tradeoff between yield and cell efficiency, to a certain extent, the resulting low-lifetime edge region close to the crucible wall is accepted in industrial mc-Si wafers, having a negative impact on the mean cell efficiency of the processing lines. It can be shown that in the as-grown state, a significant fraction of the recombination activity in the low-quality edge region, as well as in the high-quality center region of mc-Si ingots, is attributed to interstitial Fe (Fe_i) [14], [15]. However, since the dissolved iron atoms are effectively removed during standard solar cell processing, one important question is to which extent precipitated Fe atoms contribute to the experimentally assessed carrier lifetime distribution before and after gettering. Knowing about the impact of Fe precipitates on lifetime would allow for further process optimization and, thus, increased cell efficiency and yield.

In several publications, the impact of the precipitate distribution on the carrier lifetime [16], [17] was calculated via the simple approach given by del Cañizo [18], which is based on the work of Hwang and Schroder [19]. However, the treatment in [18] neglects the band bending around the metallic precipitates which is a result of the internal Schottky contact between the metal cluster and the surrounding silicon [20]–[23]. According to thermionic emission theory [24], the carrier recombination at the precipitate surface depends strongly on the parameters which also affect the electric field around the precipitate, i.e., the doping concentration, the precipitate size, the Schottky barrier height, and, in particular, the injection rate [6]. A suitable approach to estimate the impact of the internal Schottky contact between precipitate and semiconductor on the carrier recombination was introduced by Plekhanov and Tan [6]. Using 1-D finite-element method (FEM) simulations, they assessed the theoretical influence of several model parameters on the recombination properties of a mean-field distribution of iron

Manuscript received September 27, 2013; revised December 2, 2013 and January 11, 2014; accepted January 20, 2014. This work was supported in part by the German Federal Ministry for the Environment, Nature Conservation, and Nuclear Safety and in part by industry partners within the research cluster "SolarWinS" under Contract 0325270G, as well as in part by the research project "THESSO" under Contract 0325491.

W. Kwapil and F. Schindler are with the Fraunhofer Institut für Solare Energiesysteme, Freiburg 79110, Germany, and also with Freiburger Materialforschungszentrum, Albert-Ludwigs-Universität Freiburg, Freiburg 79104, Germany (e-mail: wolfram.kwapil@ise.fraunhofer.de; florian.schindler@ise.fraunhofer.de).

J. Schön, W. Warta, and M. C. Schubert are with the Fraunhofer Institut für Solare Energiesysteme, Freiburg 79110, Germany (e-mail: jonas.schoen@ise.fraunhofer.de; wilhelm.warta@ise.fraunhofer.de; martin.schubert@ise.fraunhofer.de).

Color versions of one or more of the figures in this paper are available online at http://ieeexplore.ieee.org.

Digital Object Identifier 10.1109/JPHOTOV.2014.2304355

precipitates having the same radius without comparing these results to experiments. They found that "[. . .] each of [. . .] [the] conclusions holds with the other parameters [. . .] remaining constant, and should not be excessively generalized." The difficulty in finding general conclusions is a result of the interplay between the different factors mentioned previously. For example, a small precipitate that is close to a large cluster will see a different charge carrier distribution than one neighboring another small precipitate at the same distance. As a result, the space charge regions surrounding the small cluster will differ in both cases. Hence, in order to be able to compare simulated and measured recombination at precipitates, realistic distributions of iron precipitates need to be considered. As realistic Fe precipitate dimensions extend over a wide range of sizes, we use 2-D FEM simulations to accommodate both the precipitate size distribution and the wafer geometry in one model.

In the following, the carrier lifetimes due to realistic Fe precipitate distributions before and after a phosphorus emitter diffusion in two exemplary wafer regions, i.e., the wafer edge and the center part, will be analyzed. The results will be compared with carrier lifetime measurements on neighboring passivated mc-Si wafers: one in the as-grown and one in the P-diffused state. While the lifetime in the edge region can be explained by the measured interstitial iron concentration in the *low*-injection regime, we will show that it is possible to explain the relatively small slope in $\tau_{\mathrm{eff}}(\Delta n)$ at mid to high injection by the injection-dependent recombination currents toward the iron precipitates. This conclusion is valid for both the as-grown and the diffused wafer. Therefore, our model can eventually be used to evaluate the impact of Fe precipitates on solar cell parameters (e.g., via efficiency limiting bulk analysis [25]).

II. Experimental Details and Modeling

The comparison between experimental and simulated carrier lifetime values at different positions in a standard mc-Si ingot becomes possible if the iron distributions in the dissolved, as well as in the precipitated state, are known. The measurements of the total and interstitial iron distributions in the as-grown state of the exemplary wafer used for this study, as well as details concerning the crystallization process and simulations of the temperature distribution and Fe in-diffusion are presented in detail elsewhere (block named "standard" in [26] and [14]) and shall be summarized: The mc-Si crystallization of the block (format Gen1) was performed in a standard-type crucible in a laboratory crystallization furnace at Fraunhofer ISE. The p-type resistivity is around 1 Ω·cm at mid-ingot height. Total iron concentrations at the crucible wall at 50% ingot height (the position from which the wafer was taken) were determined via inductively coupled plasma mass spectrometry (ICP-MS) to be 1–3 $\times$ 10^{15} at/cm^3 after crystallization. By following a distribution resembling an error function, the values decrease to $\sim$1 $\times$ 10^{14} at/cm^3 at a distance of 2 cm to the crucible wall and to $\sim$1 $\times$ 10^{11} at/cm^3 at 4-cm distance. Interstitial iron concentrations were measured by means of Fe_i/FeB-pairing via quasi steady state photoluminescence (QSSPL)–calibrated photoluminescence (PL) imaging [26], [27] on as-cut wafers to be around 1 $\times$ 10^{12} at/cm^3 in the edge region and around 1 $\times$ 10^{11} at/cm^3 in the center region.

Prior to the QSSPL measurements, the wafers were surface-passivated by Al_2O_3 atomic layer deposition, allowing for very low-surface recombination velocities. On FZ reference wafers, lifetimes above 1 ms in the entire injection range of interest were achieved. While we expect no influence on carrier lifetime because of passivation of defects by hydrogen atoms diffusing from the passivation layer, a slight growth of the precipitates because of the low-temperature anneal needed for surface passivation activation may have occurred, slightly increasing the carrier lifetime. However, we estimate this uncertainty to be negligible in comparison with other sources of error discussed next because of the short times needed for this process step. Care was taken to separate the Fe_i/FeB-metastability from other metastable defects like the formation of the B–O complex or the Cr_i/CrB defects by following the procedure described in [27].

A phosphorus emitter diffusion at 825 °C was applied to a neighboring wafer. After emitter etch-back and Al_2O_3 surface passivation, the interstitial iron concentration was measured to be approximately 3 $\times$ 10^{11} at/cm^3 in the edge region and $\sim$1 $\times$ 10^{10} at/cm^3 in the wafer center [15]. As the total iron concentration after diffusion could not be determined via ICP-MS, we rely on the simulations of the Fe redistribution during the high-temperature step, which will be explained in detail next.

The electron-hole recombination at the precipitate surface depends on the electric field strength and, hence—beside other factors—on the precipitate size. For our study, we thus need detailed information about the precipitate size distribution as a function of the distance to the crucible wall. Unfortunately, these data are not accessible on a statistical scale via experiments (particularly along dislocation lines crossing the wafer bulk), e.g., by means of micro-X-ray fluorescence [28]. Therefore, we use 2-D simulations (Sentaurus Process [29]), which yield—besides the Fe_i concentration—the distribution of the Fe cluster sizes (for details, see [3], [9], and [11]). As shown in [14], our simulations could reproduce the measured total and interstitial iron distributions as a function of the distance to the crucible wall in the as-grown wafer taken for this study with high accuracy.

The 2-D Fe distribution simulation is based on the diffusion equations and the Fokker–Planck equations. As input, a 2-D symmetry element containing the interface between the crucible wall and the mc-Si crystal is given together with a typical dislocation distribution [14]. The dislocations are assumed to be perpendicular to the 2-D plane. In the model, the dislocations serve as nucleation sites for Fe precipitation. In addition, the entire temperature ramp during crystallization is considered and used for the calculation of impurity in-diffusion into the melt, as well as into the solidified crystal and the nucleation and precipitation process, yielding the precipitate distribution in the as-grown state. In the calculation of the distribution after the phosphorus diffusion, in addition the gettering effect is taken into account [11]. In [3], simulation results of mc-Si in the as-grown, as well as in the phosphorus-gettered state, were compared with X-ray fluorescence microscopy (μ-XRF) measurements of Fe clusters along grain boundaries,

and a reasonable agreement was found. In addition, measured changes in Fe_i concentration because of dissolution and precipitation, as well as the gettering effects, were reproduced with simulations providing evidence for the soundness of this approach [11], [15].

Since the heterogeneous precipitation of iron depends very sensitively on the temperature history of the silicon samples, the largest contribution to the uncertainty in the predicted precipitate size density comes from the temperature ramp during crystallization. Unfortunately, direct *in-situ* temperature measurements in the bulk silicon are impossible. Hence, complex simulations of the temperature fields in the crystallization furnace and the silicon block, incorporating diffusive and convective mass transport in the melt and the atmosphere, were used for the precipitation simulations [14]. A second source of uncertainty comes from the measurement of the distance between the crucible wall and the edge of the wafer taken from approximately 50% ingot height that was used for carrier lifetime measurements, the precipitate size distribution in the wafer edge being strongly dependent on the distance to the crucible wall.

In this study, we are interested in the reasons for limitations of the carrier lifetime in the low-lifetime edge region as compared with the wafer center region. Understanding the limitations may help to optimize process sequences in order to increase the carrier lifetime in the edge region, which has severely affected the material performance up to now. The greatest lifetime enhancement is likely within the grains with low dislocation densities [1]. Therefore, in the following, we disregard grain boundaries and regions of high dislocation density $\rho_{\mathrm{DL}} \geq 10^5$ cm^{-2} and focus on the carrier lifetime inside grains (background dislocation density $\rho_{\mathrm{DL}} \sim 10^4$ cm^{-2}). Fe nucleation in grains far away from a grain boundary occurring most likely at the remaining dislocations [30], [31], we assume that the precipitates are aligned along a dislocation line traversing the entire wafer thickness. Taking a relatively low ρ_{DL} of 1×10^4 cm^{-2}, we can calculate the number of precipitates of a certain size expected to be found at the dislocation, which we use for the following calculation.

The simulations of the injection-dependent precipitate-related carrier lifetime are based on 2-D axisymmetric finite-element simulations using Comsol Multiphysics. A sketch of the model geometry and some of the basic features is presented in Fig. 1 (on the left). The simulation domain is bounded by the wafer surfaces (top and bottom), the wafer thickness being 200 μm, and the domain radius equals 56.42 μm (which corresponds to a ρ_{DL} of 10^4 cm^{-2}). The spherical precipitates of different size and number are aligned along the axis of symmetry representing the dislocation line. The precipitates are randomly distributed in size along the dislocation. Between neighboring precipitates, an equal distance is maintained. An electron-hole generation profile G correlating with AMG1.5 g spectrum illumination is used. Besides recombination at the wafer surfaces and at the precipitates, band-to-band recombination R_{BB} (parameterization from [32]), Auger recombination R_{Auger} [33], and Shockley–Read–Hall recombination at iron interstitials R_{Fei} [34] are taken into account.

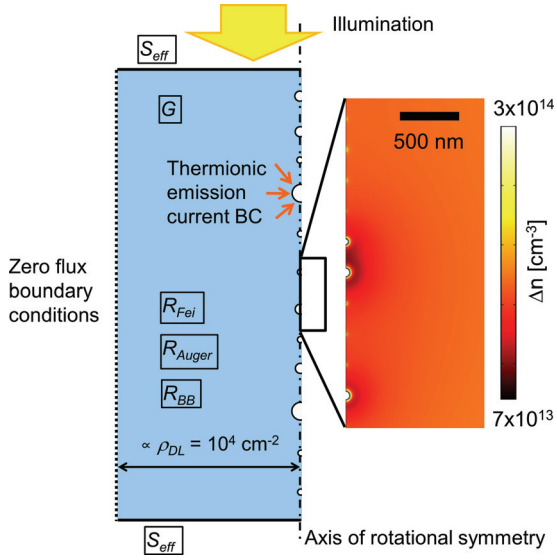

Fig. 1. Left: Sketch of the model structure (not to scale) used in the FEM simulations of recombination currents at internal Schottky contacts (thermionic emission current BCs between Fe precipitates and silicon and (right) exemplary zoom into the simulated steady-state minority carrier distribution (generation rate 1 sun), shown for the precipitate size density labeled "egde–distr. 1" (see Fig. 3). Moving from the precipitate–semiconductor interface toward the Si bulk, a minority carrier accumulation is followed by a depleted region before the bulk average minority carrier concentration is attained. Interplay between neighboring precipitates can be exemplarily seen in the overlapping minority carrier reduction in the vicinity of the two large precipitates close to the middle of the image.

The simulation is based on the approach that is presented in previous publications by Plekhanov and Tan [6] and by Negoita and Tan [35], and the details of the derivation of the boundary condition (BC) equations and the implementation can also be found in [6] and [35]. In the following, the implementation used in this study is summarized.

In the silicon bulk, the simulation solves the continuity equations for electrons and holes and the Poisson equation (assuming Maxwell–Boltzmann statistics) with the three unknown variables Φ_e, Φ_h, and Ψ, i.e., the quasi-Fermi potentials for electrons and holes and the electrostatic potential, respectively. At the wafer surfaces, recombination fluxes corresponding to a surface recombination velocity $S_{\mathrm{eff}} = 200$ cm/s are chosen as Neumann BC, while the boundaries perpendicular to the wafer surface are described by zero flux BCs, assuming lateral periodicity.

As described in [6] and [35], the interface between silicon and the metallic precipitates is assumed to represent an internal Schottky contact that is described by the Schottky barrier Φ_B. We suppose the precipitates to consist of iron silicide (FeSi) with the Schottky barrier $\Phi_B = 0.68$ eV (p-type Si) [6]. As will be shown next, realistic precipitate distributions extend over a wide range of sizes from several atoms per cluster (radius < 1 nm) to precipitate radii of several tens of nanometers. It is likely that the electronic properties and, therefore, the Schottky barrier height depend on the precipitate size for example due to quantum mechanical effects [20] or due to lattice misfit effects that induce stress for larger clusters [36]. However, for precipitates above a

certain size, we expect the change in Schottky barrier height to be relatively small, which, according to Plekhanov and Tan [6], should have a negligible impact on the recombination activity. For small precipitates with radii in the order of 0.1 to 1 nm, the change in Schottky barrier height may be significant, or the Schottky contact model may even not be valid at all. In the next section, we will show that the contribution of these precipitates to the total recombination is negligible. Hence, we expect the error that is introduced by approximating the Schottky barrier height by a single value to be small.

The Schottky contact results in thermionic emission current densities of electrons j_e and holes j_h:

$$j_e = A_e^* T^2 \exp\left(-\frac{q\Phi_B}{k_B T}\right)\left\{\exp\left(\frac{-q\Phi_e - E_{F,m}}{k_B T}\right) - 1\right\} \quad (1)$$

$$j_h = A_h^* T^2 \exp\left(-\frac{E_G - q\Phi_B}{k_B T}\right)\left\{\exp\left(\frac{q\Phi_h + E_{F,m}}{k_B T}\right) - 1\right\}. \quad (2)$$

Here, $A_{e,h}^*$ signifies the effective Richardson constants for electrons and holes, respectively, T the temperature, q the elementary charge, k_B the Boltzmann constant, E_G the band gap of silicon, and $E_{F,m}$ the Fermi level in the iron precipitates. The precipitates charge with the majority carrier species and a depletion region surrounding the metal cluster evolves, attracting minority carriers and repelling majority carriers [35]. In thermodynamic equilibrium (in the dark), the net fluxes of electrons and holes toward the precipitates are zero [35]. Under injection conditions, e.g., illumination, the strong electric fields in the depletion regions around the precipitates decrease [35]. As a consequence, both electrons and holes travel toward the precipitates where they recombine [35]. In the steady state, electron and hole current densities at the precipitate–Si interface must be in equilibrium:

$$j_e|_{\text{interface}} = j_h|_{\text{interface}}\,. \quad (3)$$

Here, it is assumed that the recombination velocity is not the limiting factor once the carriers reach the Fe precipitate surface [6].

The condition (3), together with (1) and (2), is used to derive a consistent set of BCs describing the recombination at metallic precipitates [35].

Because of the charging of the precipitates, large electric fields evolve which can reach up to several 10^6 V/cm. In particular, this is the case for small precipitates and very low injection. In this high-field regime, the carrier mobility, for which we use Klaassen's model [37], [38], has to be corrected for field effects [39].

From the primary result of these simulations—the spatial distribution of the potentials Φ_e, Φ_h, and Ψ—all necessary values can be derived. In particular, the excess minority carrier density Δn is obtained by averaging the electron concentration over the whole simulation domain. The recombination due to the precipitates is calculated by integrating the recombination currents over the interfaces of all precipitates, yielding the total recombination rate R_{prec}, which is then averaged over the whole simulation domain.

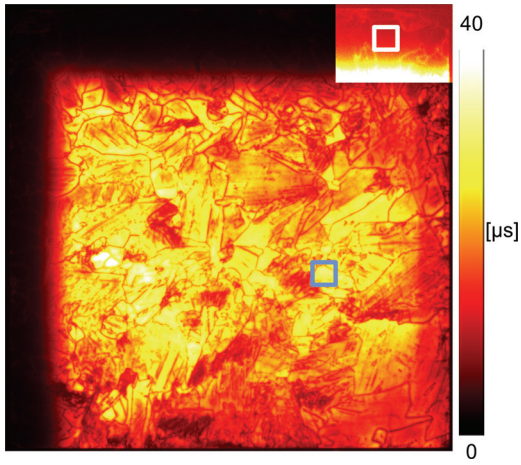

Fig. 2. Carrier lifetime at a generation rate of 0.1 sun on the passivated as-grown wafer taken from approximately 50% ingot height showing low-lifetime edge regions at the upper and left sides. Scaling is linear, 0 to 40 μs, for the image of the entire wafer. The white rectangle marks the ROI from which the measured injection-dependent carrier lifetime was extracted (see Fig. 4). In the blue rectangle, the carrier lifetime in the "center" was evaluated. The inset in the edge to the upper right is scaled to 0–5 μs in order to highlight the ROI in the edge region.

As usual, the quasi-steady state carrier lifetime $\tau_i(\Delta n)$ that is related to the recombination rate channels R_i is calculated as

$$\tau_i(\Delta n) = \frac{\Delta n}{R_i} \quad (4)$$

with i symbolizing the recombination channel.

III. Results

In Fig. 2, the QSSPL-calibrated PL image of the as-grown wafer taken for this study is shown. In both the as-grown and the phosphorus-diffused sister wafer, two exemplary regions of interest (ROI) were chosen, which are marked by the rectangles: The first one represents a grain with low dislocation density in the low-lifetime edge region that is approximately 15–20 mm away from the crucible wall. For the second ROI, a grain of relatively good crystal quality possessing a low dislocation density in the center region of the ingot was chosen. Care was taken to average only over pixels with a significant distance to the surrounding grain boundaries. In order to avoid possible influences of light-spreading effects on the carrier lifetime measurements [40] in P-diffused wafers because of the large intensity difference between center and edge, here, the high-lifetime center region was masked out, and the QSSPL measurement approach in [41] was used. In general, we estimate the carrier lifetime measurement error to be $\sim$20%.

In Fig. 3, the simulated Fe cluster size densities inside the grains in the edge ROI and in the good wafer area ROI which were taken as input for the calculation of the carrier lifetime are shown. For the evaluation, cluster sizes (number of atoms per

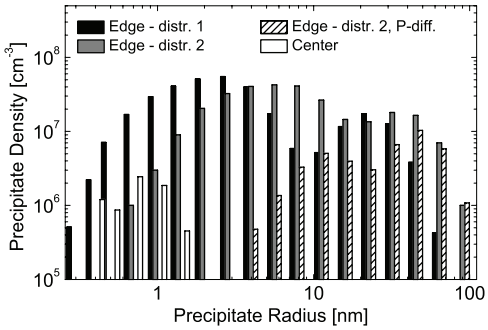

Fig. 3. Distribution of the precipitate size density within the grains in the edge before (black and gray) and after phosphorus diffusion (shaded white) as well as in the center (white) regions at 50% ingot height taken from simulations of mc-Si crystallization [10], [14]. The distribution in the edge region labeled with "distr. 1" corresponds to a grain 15–20 mm away from the crucible wall that was cooled down with the simulated temperature profile (see the marked edge region in Fig. 2). The distribution 2 represents a ROI closer to the crucible wall and was used for uncertainty estimations (see the text).

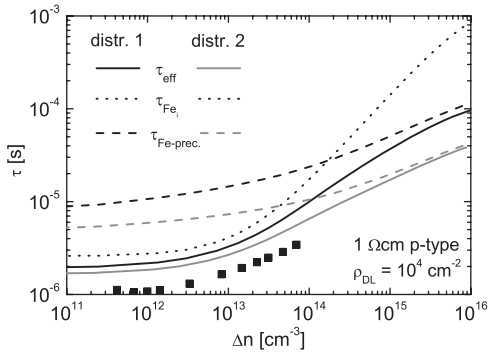

Fig. 4. Calculation of the carrier lifetime (in the dissociated state) in the edge region before phosphorus diffusion where the Fei concentration was measured to be 1×10^{12} at/cm^3. The measured increase of the carrier lifetime with the increasing injection level (black symbols) is smaller than expected if only the SRH recombination at dissolved iron atoms (dotted line) is accounted for. However, taking recombination at Fe precipitates (dashed lines) into account, the calculated effective lifetime (continuous lines) agrees well with measurements. For the explanation of the difference in gray and black lines, please refer to the text.

cluster) were binned exponentially. The four different precipitate size densities investigated in this study are detailed as follows:

1) "Edge–distr. 1" (black columns) represents the precipitate distribution inside the grains in the edge ROI in the as-grown state, 15–20 mm away from the crucible wall.
2) "Edge–distr. 2" (gray columns) features a higher density of larger Fe clusters compared with the previous distribution, which is found closer to the crucible wall because of the higher total Fe concentration. Larger precipitates may also result from a smaller cooling rate after crystallization. Hence, by this distribution variation in the as-grown state, we estimate the impact of the uncertainties in Fe precipitate distribution mentioned in the previous section.
3) "Edge–distr. 2, P-diff." (white-shaded columns) represents the simulated Fe precipitate distribution inside grains in the edge after a phosphorus emitter diffusion (gettering) step.
4) "Center" (white columns) stands for a typical simulated Fe cluster distribution inside grains in the good wafer area far away from the crucible wall.

While the Fe in-diffusion from crucible and coating during the cool down leads to a high precipitate density and to a significant fraction of large precipitates in the edge region, in the ingot center, only few and relatively small precipitates are to be expected. During the phosphorus diffusion, the change in the Fe cluster distribution depends strongly on the precipitate size: While small precipitates are effectively dissolved because of the high temperature, large precipitates are hardly affected. After P-diffusion, most of the dissolved iron atoms are gettered or reprecipitated at the remaining clusters.

An example for the simulated steady-state minority carrier distribution taking the thermionic emission currents into account is presented in Fig. 1 (on the right). Depending on the precipitate size density and the properties which have an influence on the electric field, precipitates can interact via overlapping space charge regions.

The measurements of the injection-dependent carrier lifetime that is averaged according to a square-root harmonic mean within the edge ROI before P-diffusion are presented in Fig. 4. The lifetime in the edge region increases from 1 μs in low injection to 3 μs in the mid-injection range. These experimental values can only partly be explained by SRH recombination at iron interstitials of the measured (and simulated [14]) concentrations of 1×10^{12} at/cm^3 in this region. In particular, in the mid- to high-injection regime, significant deviations occur.

As shown in Fig. 4, the calculated recombination at Fe precipitates (dashed lines) shows a notable injection dependence, which has a slighter slope than the SRH recombination channel for Fe$_i$. With the Fe-precipitate size distribution expected for the edge part of the ingot, our calculations show that recombination at precipitates dominates the carrier lifetime starting at an injection level of around 5×10^{13} to 1×10^{14} cm^{-3}. Hence, one possible explanation for the relatively slow increase in measured effective carrier lifetime in mid- to high-injection is the presence of Fe clusters.

The difference between measurement and simulation with the second set (grey continuous line) amounts to 0.5–1.5 μs (for 1×10^{11} cm$^{-3} < \Delta n < 1 \times 10^{14}$ cm^{-3}) and remains small. In this example, only a small fraction of the measured total recombination at additional centers, apart from iron-related ones, has to be assumed in order to reach perfect agreement. The good agreement, supposing a higher concentration of large precipitates, gives support to the hypothesis that the injection-dependent lifetime in the edge region can be attributed in a large part to recombination at iron interstitials (being prominent in the low-injection range) and recombination at Fe precipitates (important in the mid- to high-injection range).

Of course, also other impurities like Cu, Ni, O, etc., are present in the wafer. However, the carrier lifetime distribution as a function of the distance to the crucible wall follows a profile that provides a fingerprint of the diffusion length (dependent on crystallization conditions) of the limiting defect. The distribution of most other impurities is different because of their different diffusivity; for example, the concentration of Cu and Ni is

laterally almost homogeneous [13] because of their large diffusion length [42], which levels out any gradients during cooldown. Therefore, the impact of these elements on carrier lifetime can theoretically be observed in the wafer center region as well. Since the carrier lifetimes in the wafer center and the edge differ strongly, it is unlikely that these impurities contribute significantly to the lifetime limitation in the wafer edge region. This line of reasoning applies to most of other impurity elements [42]. Of course, our measurements in the wafer edge ROI still contain the influence of impurities with diffusivity similar to Fe, like, e.g., Cr, which are not regarded in the simulations.

During measurements of the dissolved Fe concentration via the Fe_i/FeB metastability [43], the injection dependence of precipitate-related lifetime needs to be considered if the Fe concentration is high and the precipitate density is significant (in particular in the wafer edge regions). Since the [Fe_i] evaluation assumes that the measured effective lifetime has no other injection dependence than one introduced by the Fe_i/FeB defect, it is advisable to choose an injection level in which the precipitate-related carrier lifetime is almost constant. Our simulations suggest this to be the case at low-minority carrier densities roughly below 5×10^{12} cm^{-3}.

Comparing our results to previous approximations of the precipitate-related carrier lifetime, the estimation that is based on the equations in [18] and [19] for the precipitate size distributions yields 44.4 μs and 14.9 μs for distributions 1 and 2, respectively. In our calculations, these values are expected to be found only at an injection level around 5×10^{14} cm^{-3} (corresponding to $\sim$1.7 and $\sim$3 suns, respectively), with significantly lower lifetime values at lower injection. Depending on the injection conditions, the values that were estimated by the approach in [18] may differ from the real values by an order of magnitude. The reason is that the simple approach neglects the space charge region around the precipitates, which also depends on the injection conditions.

During phosphorus diffusion, in the edge region, small precipitates are effectively dissolved, and a large part of the interstitial iron atoms are gettered (the remaining Fe_i concentration being approx. 3×10^{11} at/cm^3). However, with increasing precipitate size, the effect of the P-diffusion decreases. The resulting simulations of the carrier lifetime after P-diffusion, as well as the measured lifetime on the P-diffused sister wafer, are shown in Fig. 5. The simulation is in reasonable agreement with the measured lifetime, which increases during P-diffusion by a factor of $\sim$2–3, depending on injection density. Again, we attribute the deviation between simulation and measurement mainly to the uncertainty in the precipitate size distribution. While Fe interstitials still play a significant role in the low-injection regime, the precipitates mainly limit the carrier lifetime above an injection level $>1 \times 10^{13}$ cm^{-3}. After P-diffusion, the relative impact of Fe precipitates on lifetime increases strongly compared with the as-grown state, because of the lower Fe_i concentration. For example, at an injection level of 1×10^{14} cm^{-3}, from our calculations, we estimate the share of recombination at precipitates to be roughly 40% of the total recombination before P-diffusion. After emitter diffusion, we attribute about 70% of the total recombination to the influence of Fe precipitates. This example shows how important it is to consider the effect of Fe precipitates in the edge region during solar cell processing.

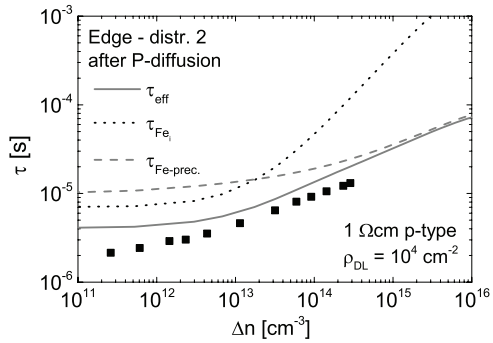

Fig. 5. Calculation of the carrier lifetime after phosphorus diffusion in the edge region ($Fe_i \sim 3 \times 10^{11}$ at/cm^3) assuming the precipitate distribution 2. The simulation shows the same trend as the lifetime measurement (black symbols), indicating that in the wafer edge, the remaining precipitates may play a significant role.

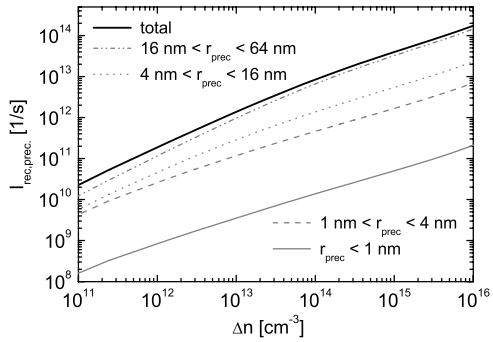

Fig. 6. Injection-dependent recombination current for precipitates with different sizes, exemplarily shown for the precipitate distribution 1. The gray lines represent the recombination currents integrated over all precipitates with sizes mentioned in the legend. Recombination at the large precipitates is predominant; hence, in principle, precipitates with radii <4 nm can be neglected. The black continuous line represents the total precipitate-related recombination current.

In the good wafer region inside the grains, we calculate a Fe precipitate-related lifetime above 1 ms (not shown), which means that Fe precipitates of the simulated size distribution labeled "center" in Fig. 3 do not affect the carrier lifetime independent of the injection density. The measured lifetimes in the as-grown state can be well explained by recombination at iron interstitials at least in the low- to mid-injection regime. A difference between measured effective carrier lifetime and Fe_i recombination in the mid- to high-injection range is observed, which we attribute to other background defects.

A deeper analysis of the four exemplary simulations presented previously reveals that at least for the precipitate distributions assumed herein, recombination at large precipitates is predominant, where the influence of small precipitates with radii roughly below 4 nm is negligible (see Fig. 6). This explains the noticeable difference between precipitate distributions of significantly different sizes (edge–distr. 1 and 2; see Fig. 4). Obtaining a large lifetime increase in the wafer edge region by a simple phosphorus emitter diffusion/gettering is challenging because large precipitates are the most difficult to getter and, at the same time, have the largest impact on lifetime.

IV. Conclusion

Metal precipitates in mc-Si, with iron clusters being the most prominent of all because of the high Fe concentration in the crucible and coating, significantly reduce the carrier lifetime, the metallic silicides likely forming an internal Schottky contact with the surrounding silicon. The resulting thermionic emission currents (recombination currents) depend on all parameters which have an impact on the electric field around the precipitates, in particular the injection level.

Our simulations of realistic precipitate size densities and recombination of charge carriers at precipitates at a low dislocation density show that a possible explanation for the measured injection-dependent carrier lifetime is that in the mid- to high-injection range in the grains of the edge region close to the crucible wall is limited by recombination at iron precipitates, while SRH recombination at iron interstitials plays a crucial role only at low injection. Our results therefore indicate that the internal Schottky contact at the iron precipitate interfaces has to be taken into account in order to understand and predict the injection-dependent carrier lifetime at least in the wafer edge correctly. Calculations of precipitate-related recombination inside the grains in the wafer edge after a phosphorus diffusion step, which leads to the dissolution of the small precipitates and gettering of most of the interstitial iron and, thus, to a slight lifetime increase, are also in good accordance with measurements.

In our simulations, the precipitate-related recombination is dominated by the large precipitates with radii >4 nm. Since large iron clusters are hardly dissolved during standard gettering steps, their relative impact on the lifetime increases considerably during processing.

Within grains in the wafer center, no impact of Fe clusters on carrier lifetime is expected.

By combining realistic simulations of the precipitate size density evolution during crystallization and processing with calculations of the recombination at the precipitate surfaces, we are now able to estimate the impact of various process sequences on one of the most important material parameters in solar cell processing: the carrier lifetime (diffusion length).

Acknowledgment

The authors would like to thank A. Abdollahinia for assistance with the precipitate distribution simulations, as well as L. Mundt and J. Giesecke for the carrier lifetime measurements.

References

[1] A. Bentzen, A. Holt, R. Kopecek, G. Stokkan, J. S. Christensen, and B. G. Svensson, "Gettering of transition metal impurities during phosphorus emitter diffusion in multicrystalline silicon solar cell processing," *J. Appl. Phys.*, vol. 99, pp. 093509-1–093509-6, 2006.

[2] D. P. Fenning, J. Hofstetter, M. I. Bertoni, S. Hudelson, M. Rinio, J. F. Lelièvre, B. Lai, C. Del Cañizo, and T. Buonassisi, "Iron distribution in silicon after solar cell processing: Synchrotron analysis and predictive modeling," *Appl. Phys. Lett.*, vol. 98, pp. 162103-1–162103-3, 2011.

[3] J. Schön, A. Haarahiltunen, H. Savin, D. P. Fenning, T. Buonassisi, W. Warta, and M. C. Schubert, "Analyses of the evolution of iron-silicide precipitates in multicrystalline silicon during solar cell processing," *IEEE J. Photovoltaics*, vol. 3, no. 1, pp. 131–137, Jan. 2013.

[4] D. P. Fenning, J. Hofstetter, M. I. Bertoni, G. Coletti, B. Lai, C. Del Cañizo, and T. Buonassisi, "Precipitated iron: A limit on gettering efficacy in multicrystalline silicon," *J. Appl. Phys.*, vol. 113, pp. 044521-1–044521-12, 2013.

[5] T. Buonassisi, A. A. Istratov, M. A. Marcus, B. Lai, Z. Cai, S. M. Heald, and E. R. Weber, "Engineering metal-impurity nanodefects for low-cost solar cells," *Nat. Mater. Lett.*, vol. 4, pp. 676–679, 2005.

[6] P. S. Plekhanov and T. Y. Tan, "Schottky effect model of electrical activity of metallic precipitates in silicon," *Appl. Phys. Lett.*, vol. 76, no. 25, pp. 3777–3779, 2000.

[7] A. Haarahiltunen, H. Väinölä, O. Anttila, E. Saarnilehto, M. Yli-Koski, J. Storgårds, and J. Sinkkonen, "Modeling of heterogeneous precipitation of iron in silicon," *Appl. Phys. Lett.*, vol. 87, pp. 151908-1–151908-4, 2005.

[8] A. Haarahiltunen, H. Väinölä, and M. Yli-Koski, "Modeling and optimization of internal gettering of iron in silicon," *ECS Trans.*, vol. 3, no. 4, pp. 273–284, 2006.

[9] A. Haarahiltunen, H. Väinölä, O. Anttila, M. Yli-Koski, and J. Sinkkonen, "Experimental and theoretical study of heterogeneous iron precipitation in silicon," *J. Appl. Phys.*, vol. 101, pp. 043507-1–043507-6, 2007.

[10] J. Schön, H. Habenicht, M. C. Schubert, and W. Warta, "Simulation of iron distribution after crystallization of mc silicon," *Solid State Phenomena*, vol. 156–158, pp. 223–228, 2010.

[11] J. Schön, H. Habenicht, M. C. Schubert, and W. Warta, "Understanding the distribution of iron in multicrystalline silicon after emitter formation: theoretical model and experiments," *J. Appl. Phys.*, vol. 109, pp. 063717-1–063717-8, 2011.

[12] D. Macdonald, A. Cuevas, A. Kinomura, Y. Nakano, and L. J. Geerligs, "Transition-metal profiles in a multicrystalline silicon ingot," *J. Appl. Phys.*, vol. 97, pp. 033523-1–033523-7, 2005.

[13] W. Kwapil, A. Zuschlag, I. Reis, I. Schwirtlich, S. Meyer, R. Zierer, R. Krain, F. K. Kießling, M. Schumann, C. Schmid, and S. Riepe, "Influence of crucible and coating on the contamination of directionally solidified silicon: First results of the German research network SolarWinS," in *Proc. 27th Eur. Photovoltaics Sol. Energy Conf. Exhib.*, Frankfurt, Germany, 2012, pp. 627–635.

[14] M. C. Schubert, J. Schön, F. Schindler, W. Kwapil, A. Abdollahinia, B. Michl, S. Riepe, C. Schmid, M. Schumann, S. Meyer, and W. Warta, "Impact of impurities from crucible and coating on mc-silicon quality—The example of iron and cobalt," *IEEE J. Photovoltaics*, vol. 3, no. 4, pp. 1250–1258, Oct. 2013.

[15] F. Schindler, B. Michl, J. Schön, W. Kwapil, W. Warta, and M. C. Schubert, "Solar cell efficiency losses due to impurities from the crucible in multicrystalline silicon," *IEEE J. Photovoltaics*, vol. 4, no. 1, pp. 122–129, Jan. 2014.

[16] M. C. Schubert, J. Schön, B. Michl, A. Abdollahinia, and W. Warta, "Modeling distribution and impact of efficiency limiting metallic impurities in silicon solar cells," in *Proc. IEEE 38th Photovoltaic Spec. Conf.*, Austin, TX, USA, 2012, pp. 286–291.

[17] M. C. Schubert, J. Schön, B. Michl, A. Abdollahinia, and W. Warta, "Advances in characterization and modeling of efficiency limiting impurities in silicon solar cells," presented at the 6th Int. Symp. Adv. Sci. Technol Silicon Mater., Kona, HI, USA, Nov. 19–23, 2012.

[18] C. Del Cañizo and A. Luque, "A comprehensive model for the gettering of lifetime-killing impurities in silicon," *J. Electrochem. Soc.*, vol. 147, no. 7, pp. 2685–2692, 2000.

[19] J. M. Hwang and D. K. Schroder, "Recombination properties of oxygen-precipitated silicon," *J. Appl. Phys.*, vol. 59, pp. 2476–2487, 1986.

[20] A. Broniatowski, "Multicarrier trapping by copper microprecipitates in silicon," *Phys. Rev. Lett.*, vol. 62, pp. 3074–3077, 1989.

[21] C. Donolato, "The space-charge region around a metallic platelet in a semiconductor," *Semicond. Sci. Technol.*, vol. 8, pp. 45–49, 1993.

[22] P. Formanek and M. Kittler, "Direct evidence of internal Schottky barriers at NiSi2 precipitates in silicon by electron holography," *J. Appl. Phys.*, vol. 97, pp. 063707-1–063707-5, 2005.

[23] M. Kittler, J. Lärz, W. Seifert, M. Seibt, and W. Schröter, "Recombination properties of structurally well defined $NiSi_2$ precipitates in silicon," *Appl. Phys. Lett.*, vol. 58, pp. 911–913, 1991.

[24] C. Herring and M. H. Nichols, "Thermionic emission," *Rev. Mod. Phys.*, vol. 21, no. 2, pp. 185–270, 1949.

[25] B. Michl, M. Rüdiger, J. Giesecke, M. Hermle, W. Warta, and M. C. Schubert, "Efficiency limiting bulk recombination in multicrystalline silicon solar cells," *Sol. Energy Mater. Sol. Cells*, vol. 98, pp. 441–447, 2012.

[26] D. Macdonald, J. Tan, and T. Trupke, "Imaging interstitial iron concentrations in boron-doped crystalline silicon unsing photoluminescence," *J. Appl. Phys.*, vol. 103, pp. 073710-1–073710-7, 2008.
[27] M. C. Schubert, H. Habenicht, and W. Warta, "Imaging of metastable defects in silicon," *IEEE J. Photovoltaics*, vol. 1, no. 2, pp. 168–173, Oct. 2011.
[28] M. I. Bertoni, D. P. Fenning, M. Rinio, V. Rose, M. Holt, J. Maser, and T. Buonassisi, "Nanoprobe X-ray fluorescence characterization of defects in large-area solar cells," *Energy Environ. Sci.*, vol. 4, pp. 4252–4257, 2011.
[29] *Sentaurus TCAD*, Synopsys, Zürich, Switzerland, 2010.
[30] J. Bailey, S. A. McHugo, H. Hieslmair, and E. R. Weber, "Efficiency-limiting defects in silicon solar cell material," *J. Electron. Mater.*, vol. 25, pp. 1417–1421, 1996.
[31] S. A. McHugo, A. C. Thompson, G. Lamble, C. Flink, and E. R. Weber, "Metal impurity precipitates in silicon: chemical state and stability," *Physica B*, vol. 273–274, pp. 371–374, 1999.
[32] M. A. Green, *Solar Cells: Operating Principles, Technology And System Applications*. Kensington, Australia: Univ. New South Wales, 1986, ch. 3, p. 52.
[33] J. Dziewior and W. Schmid, "Auger coefficients for highly doped and highly excited silicon," *Appl. Phys. Lett.*, vol. 31, pp. 346–348, 1977.
[34] A. A. Istratov, H. Hieslmair, and E. R. Weber, "Iron and its complexes in silicon," *Appl. Phys. A, Mater. Sci. Process.*, vol. 69, pp. 13–44, 1999.
[35] M. D. Negoita and T. Y. Tan, "Metallic precipitate contribution to generation and recombination currents in p-n junction devices due to the Schottky effect," *J. Appl. Phys.*, vol. 94, pp. 5064–70, 2003.
[36] J. D. Murphy, K. Bothe, M. Olmo, V. V. Voronkov, and R. J. Falster, "The effect of oxide precipitates on minority carrier lifetime in p-type silicon," *J. Appl. Phys.*, vol. 110, pp. 053713-1–053713-9, 2011.
[37] D. B. M. Klaassen, "A unified mobility model for device simulation—I. Model equations and concentration dependence," *Solid State Electron.*, vol. 35, pp. 953–959, 1992.
[38] D. B. M. Klaassen, "A unified mobility model for device simulation—II. Temperature dependence of carrier mobility and lifetime," *Solid State Electron.*, vol. 35, pp. 961–967, 1992.
[39] C. Canali, G. Majni, R. Minder, and G. Ottaviani, "Electron and hole drift velocity measurements in silicon and their empirical relation to electric field and temperature," *IEEE Trans. Electron Devices*, vol. ED-22, no. 11, pp. 1045–1047, Nov. 1975.
[40] D. Walter, A. Fell, E. Franklin, D. Macdonald, B. Mitchell, and T. Trupke, "The impact of Silicon CCD photon spread on quantitative analyses of luminescence images," *IEEE J. Photovoltaics*, vol. 4, no. 1, pp. 368–373, Jan. 2014.
[41] J. A. Giesecke, T. Niewelt, M. Rüdiger, M. Rauer, M. C. Schubert, and W. Warta, "Broad range injection-dependent minority carrier lifetime from photoluminescence," *Sol. Energy Mater. Sol. Cells*, vol. 102, pp. 220–224, 2012.
[42] K. Graff, *Metal Impurities in Silicon-Device Fabrication*, 2nd ed. Berlin, Germany: Springer, 2000.
[43] G. Zoth and W. Bergholz, "A fast, preparation-free method to detect iron in silicon," *J. Appl. Phys.*, vol. 67, pp. 6764–6771, 1990.

Authors' photographs and biographies not available at the time of publication.